Am J Cancer Res 2026;16(2):578-592
www.ajcr.us /ISSN:2156-6976/ajcr0169084

*Original Article*

# DLGAP5 promotes salivary adenoid cystic carcinoma proliferation and metastasis through PI3K/AKT pathway

Chen-Xing Hou*, Meng-Yao Leng*, Jing-Yi Luo*, Si-Min Wang, Yuan Liu, Yue Li, Xiu-Hong Weng, Bo Cheng

*Department of Stomatology, Zhongnan Hospital of Wuhan University, 169 Donghu Road, Wuhan 430071, Hubei, China. *Equal contributors.*

Received September 29, 2025; Accepted February 3, 2026; Epub February 15, 2026; Published February 28, 2026

**Abstract:** To elucidate the oncogenic role of DLGAP5 in salivary adenoid cystic carcinoma (SACC), we characterized its expression patterns and functional impact on malignant phenotypes including proliferation, migration, and invasion; we assessed DLGAP5 expression using the GEO database, examined its effects on SACC cells through DLGAP5 knockdown and overexpression experiments, verified these findings with a nude mouse subcutaneous tumor model, and employed virtual screening to identify the lead compound ZINC3809191 targeting DLGAP5, whose inhibitory effects on SACC were confirmed in vitro. Our results showed that DLGAP5 was highly expressed in SACC and correlated with clinical stage and pathological grade, and it promoted the proliferation, migration, and invasion of SACC cells via the PI3K/AKT signaling pathway; additionally, the lead compound ZINC3809191 demonstrated significant ability to inhibit the proliferation, migration, and invasion of SACC cells. Collectively, our findings indicate that DLGAP5 is upregulated in SACC, associated with clinical stage and pathological grade, and plays a regulatory role in key malignant phenotypes of SACC cells, while the identification of ZINC3809191 with potent anti-tumor activity against DLGAP5 provides a crucial theoretical foundation for the development of potential therapeutic strategies for SACC.

**Keywords:** DLGAP5, salivary gland adenoid cystic carcinoma, virtual screening, proliferation, migration

## Introduction

Salivary gland adenoid cystic carcinoma (SACC) usually originates from the salivary glands and is characterized by a high recurrence rate, despite active local treatment [1]. The clinical prognosis for SACC remains generally poor [2], with a significant risk of distant metastasis [3], particularly to the lungs [4]. Histologically, SACC is characterized with epithelial and myoepithelial differentiated cells [5], and the ratio of myoepithelial cells to epithelial cells is a determinant of the tumor growth rate [6]. The 10-year overall survival rate of patients with SACC is approximately 29% to 37% [7], and the median survival time of patients with pulmonary metastatic SACC is only 20-32 months [8, 9]. So far, there is no effective treatment for metastatic SACC [10], making the investigation of its underlying mechanisms a critical area of research in this domain.

Discs large homolog-associated protein 5 (DLGAP5) in chromosome 14q22.3 [11] is regarded as a cell cycle regulatory protein [12]. During mitosis, it stabilizes kinetochore fibers (K-fibers) and promotes chromosome aggregation by regulating Kif18A on the centromere microtubules, playing a crucial role in the regulation of the M-phase of the cell cycle [13]. It is highly expressed in ovarian cancer [14], and its high expression is associated with poor survival prognosis [15]. Furthermore, the expression of DLGAP5 is regulated through methylation, with its up-regulation promoting hepatocellular carcinoma cells tumorigenesis via promoting cell proliferation [16]. Among endometrial cancer, DLGAP5 is highly expressed [17], and serves as a prognostic biomarker [18]. In endometrial cancer, DLGAP5 knockdown inhibits Wnt/β-catenin signaling, reduces proliferation, induces apoptosis, and impede invasive capabilities [19]. A recent genome-scale analysis reveals that DLGAP5 is significantly overexpressed in lung cancer samples [20] and has the ability to diagnose lung cancer and predict prognosis [21], and indicates that it plays a crucial role in the development of lung cancer [22]. In conclu-

https://doi.org/10.62347/XDTQ6840

sion, DLGAP5 is significantly involved in the biological processes of invasion [23], apoptosis [15], and epithelial-mesenchymal transition (EMT) [24], which contribute to the development of malignant tumors in various cancer [25, 26]. However, the role of DLGAP5 in SACC remains unclear.

Structure-based virtual screening is a rapid, efficient, and economical method widely employed in modern drug discovery [27, 28]. The utilization of advanced computer simulation technology empowers the screening and prediction of compounds exhibiting a robust binding affinity with established molecular targets, thereby facilitating the identification of potential therapeutic agents [29]. The LSD1 inhibitor SP-2577, which was determined through structure-based virtual screening, has been approved by the US Food and Drug Administration (FDA) for the treatment of Ewing's sarcoma [30]. In addition, CC-90011 has advanced to the clinical trial stage for the treatment of prostate cancer, small cell lung cancer, and other indications [31]. In our study, structure-based virtual screening approach was employed to identify potential inhibitors of DLGAP5. Consequently, our research has identified ZINC380-9191 as a novel and promising DLGAP5 inhibitor, providing valuable clues for the rational design of DLGAP5-targeted therapies.

This study investigated the role of DLGAP5 in SACC through online databases and gene knockdown. These findings indicated that DLGAP5 is highly expressed in SACC and is correlated with clinical stage and pathological grade, playing a regulatory role in cell proliferation, migration and invasion. Mechanistically, the knockdown of DLGAP5 significantly reduced the proliferation, migration and invasion of SACC-83 and SACC-LM cells by reducing the activity of PI3K/AKT signaling. Furthermore, through virtual screening, we identified DLGAP5-targeting compounds capable of suppressing SACC. These results not only establish DLGAP5 as a key oncogenic driver in SACC but also provide a pharmacological strategy for targeted intervention.

## Materials and methods

### *GEO database retrieval and DEGs identification*

The data were obtained from the Gene Expression Omnibus (GEO) database (https://www.ncbi.nlm.nih.gov/geo/). Two datasets of surgical samples of SACC and normal salivary gland tissues were obtained, including GSE88-804 and GSE153002. In order to identify the different genes at the intersection of the two datasets, the RobustRankAggreg package was used to sort the results of the differential analysis by the RRA method to obtain the differential genes at the intersection of the two datasets. The logFC absolute value greater than 1 and the corrected *p* value less than 0.05 were used to screen 747 differential genes. The utilisation of the heatmap package is imperative for the visualisation of the top 20 up-regulated and down-regulated genes.

In order to address the issue of inadequate samples for statistical analysis, the datasets were consolidated and the SVA (Surrogate Variable Analysis) package was employed to debatch the merged expression data. The screening of differentially expressed genes was conducted in accordance with the absolute value of logFC greater than 1 and the corrected *P* value less than 0.05. A total of 1739 differentially expressed genes were screened.

### *Human tissue samples*

SACC tissues and normal salivary gland tissues were obtained from the Department of Oral and Maxillofacial Surgery at Zhongnan Hospital of Wuhan University (ZNWH). The Institutional Ethics Review Board provided prior authorization for this research. All participants provided written informed consent, thereby ensuring adherence to ethical standards.

### *Cell lines*

Human SACC cell lines, including SACC-83 and SACC-LM, were obtained from Central Laboratory, Peking University School of Stomatology (Beijing, China). All cells were cultivated in complete medium comprising 10% fetal bovine serum (FBS) and 1% (100 mg/ml) penicillin/streptomycin in an incubator with a 5% $CO_2$ atmosphere at 37°C.

### *RNA extraction and RT-qPCR*

Total RNA extraction was performed using TrizolTM reagent (Invitrogen), and the concentration was subsequently measured using the Nano DropTM ND-1000. The TransScript® Two-Step RT-PCR SuperMix (TransGen Biotech) was

**Table 1.** Primer sequences for qRT-PCR

| | |
|---|---|
| GAPDH-F | 5'-CATCTCTGCCCCCTCTGCTGA-3' |
| GAPDH-R | 5'-GGATGACCTTGCCCACAGCCT-3' |
| CENPF-F | 5'-CTCTCCCGTCAACAGCGTTC-3' |
| CENPF-R | 5'-GTTGTGCATATTCTTGGCTTGC-3' |
| TTK-F | 5'-GTGGAGCAGTACCACTAGAAATG-3' |
| TTK-R | 5'-CCCAAGTGAACCGGAAAATGA-3' |
| CDK1-F | 5'-TGGGAAGTTGGTAGCTCTGAA-3' |
| CDK1-R | 5'-CCAGGGTGCTTGTCCATGTA-3' |
| CEP55-F | 5'-AGTAAGTGGGGATCGAAGCCT-3' |
| CEP55-R | 5'-CTCAAGGACTCGAATTTTCTCCA-3' |
| NUF2-F | 5'-GGAAGGCTTCTTACCATTCAGC-3' |
| NUF2-R | 5'-GACTTGTCCGTTTTGCTTTTGG-3' |
| KIF20A-F | 5'-TGCTGTCCGATGACGATGTC-3' |
| KIF20A-R | 5'-AGGTTCTTGCGTACCACAGAC-3' |
| CCNA2-F | 5'-CGCTGGCGGTACTGAAGTC-3' |
| CCNA2-R | 5'-GAGGAACGGTGACATGCTCAT-3' |
| KIF11-F | 5'-TCCCTTGGCTGGTATAATTCCA-3' |
| KIF11-R | 5'-GTTACGGGGATCATCAAACATCT-3' |
| ASPM-F | 5'-GGCCCTAGACAACCCTAACGA-3' |
| ASPM-R | 5'-AGCTTGGTGTTTCAGAACATCA-3' |
| BUB1B-F | 5'-AAATGACCCTCTGGATGTTTGG-3' |
| BUB1B-R | 5'-GCATAAACGCCCTAATTTAAGCC-3' |
| CENPE-F | 5'-GATTCTGCCATACAAGGCTACAA-3' |
| CENPE-R | 5'-TGCCCTGGGTATAACTCCCAA-3' |
| NCAPG-F | 5'-GAGGCTGCTGTCGATTAAGGA-3' |
| NCAPG-R | 5'-AACTGTCTTATCATCCATCGTGC-3' |
| DLGAP5-F | 5'-AAGTGGGTCGTTATAGACCTGA-3' |
| DLGAP5-R | 5'-TGCTCGAACATCACTCTCGTTAT-3' |
| BUB1-F | 5'-GCACCGACAATTCCAAGCTC-3' |
| BUB1-R | 5'-TGTGCTTCGTTGTGGTACAGA-3' |
| TPX2-F | 5'-ATGGAACTGGAGGGCTTTTTC-3' |
| TPX2-R | 5'-TGTTGTCAACTGGTTTCAAAGGT-3' |
| TOP2A-F | 5'-ACCATTGCAGCCTGTAAATGA-3' |
| TOP2A-R | 5'-GGGCGGAGCAAAATATGTTCC-3' |
| NUSAP1-F | 5'-AGCCCATCAATAAGGGAGGG-3' |
| NUSAP1-R | 5'-ACCTGACACCCGTTTTAGCTG-3' |
| CCNB2-F | 5'-CCGACGGTGTCCAGTGATTT-3' |
| CCNB2-R | 5'-TGTTGTTTTGGTGGGTTGAACT-3' |
| MELK-F | 5'-TCTCCCAGTAGCATTCTGCTT-3' |
| MELK-R | 5'-TGATCCAGGGATGGTTCAATAGA-3' |
| KIF23-F | 5'-AGTCAGCGAGAGCTAAGACAC-3' |
| KIF23-R | 5'-GGTTGAGTCTGTAGCCCTCAG-3' |

utilised for the synthesis of cDNA, while the PerfectStart® Green qPCR SuperMix (TransGen Biotech) was employed for qRT-qPCR. Relative gene expression levels were calculated using the comparative threshold cycle (2-ΔΔCT) method with GAPDH as endogenous control. The primer sequences corresponding to the aforementioned genes are presented in **Table 1**.

*Library preparation, sequencing, and bioinformatics analysis*

Library preparation (Illumina® Stranded mRNA Prep Kit) and sequencing (NovaSeq X Plus, 2×150 bp) were performed by Hangzhou Cosmos Wisdom Biotech. Raw reads were trimmed with fastp, aligned to the reference genome via HISAT2, and assembled using StringTie. Gene expression was quantified by RSEM (TPM), with differential expression genes (DEGs) identified via DESeq2/DEGseq ($|\log2FC| \geq 1$, FDR $\leq$ 0.05/0.001). GO/KEGG functional enrichment analyses were conducted using Goatools and KOBAS, and alternative splice events were detected with rMATS. RNA-seq data analyzed in this study can be obtained from NCBI (https://submit.ncbi.nlm.nih.gov/subs/sra/), PRJNA1379690.

*Western blot*

Protein separation was conducted via SDS-PAGE, followed by electrical transfer to a polyvinylidene fluoride membrane. The samples were blocked with a 5% skimmed milk solution for a period of two hours at room temperature. Thereafter, they were transferred and incubated in a primary antibody solution at 4°C for a period of 12 hours. The utilisation of an enhanced chemiluminescence (ECL) kit is a method of detecting blots.

*Colony formation assay*

Different groups of SACC-83 and SACC-LM cells were inoculated in 6-well plates for a period of 14 days (1000 cells/well) with medium renewal every 3 days. The cells were then fixed with 4% paraformaldehyde and stained with 0.3% crystal violet for a period of 30 minutes.

*Wound healing assay*

SACC cells were plated in six-well plates. Upon attaining a cell fusion rate of 95%, linear incisions were meticulously crafted using the precision tip of a 200 μl pipette. The cells were cultivated in serum-free medium for a period of 24 hours. The images were obtained using inverted microscopes at 0 and 24 hours.

*Animal experiments*

4-week-old female BALB/c nude mice were purchased from Wuhan WOJX BIO-TECHNOLOGY. Mice were housed within an SPF-grade animal facility, placed in individually ventilated cages (IVCs). The environmental conditions were strictly controlled at 22-25°C and a relative humidity of 40-60%, while the mice had unrestricted access to sterilized rodent chow and filtered drinking water. Regular health monitoring was conducted, and environmental enrichment measures - including nesting substrates and chew toys - were provided to safeguard the mice's welfare and alleviate stress responses.

The Animal Welfare Ethics Committee of Zhongnan Hospital of Wuhan University has granted ethical approval to all animal studies. Stable sh-NC cells and sh-DLGAP5 cells ($1\times10^7$ cells) were subcutaneously injected into 4-week-old female BALB/c nude mice. Three weeks later, the mice were euthanised and the volume and weight of the tumour were measured. Mice were first anesthetized with 5% isoflurane to a state of deep unconsciousness, followed by cervical dislocation performed by well-trained personnel. Death was subsequently confirmed by the cessation of respiration and cardiac activity. The calculation formula is as follows: The volume of the tumour is calculated using the following formula: tumor volume ($mm^3$) = (length × $width^2$)/2.

In the context of drug treatment, SACC-83 cells and SACC-LM cells ($1\times10^7$ cells) were injected subcutaneously into 4-week-old female BALB/c nude mice (obtained from GemPharmatech). The mice were treated intraperitoneally with abiraterone (0.5 mmol/kg) once a day for a period of two weeks. Subsequent to the completion of the treatment regimen, the mice were euthanised and the volume and weight of the tumour were measured.

*Virtual screening*

Virtual Screening (VS) is a significant technique in the field of computer-aided drug design, which is typically employed to screen a substantial number of chemical library molecules and identify potential drug candidate molecules. The 5,903 small-molecule compounds in the world database were retrieved and extracted in mol2 format. Thereafter, the mol2 format files were converted to pdbqt format files using the prepare_ligand4.py function within the MGTOOLS software suite. Protein: The three-dimensional structure of the protein was constructed using Alphfold3, and then dehydrated and hydrogenated in Autodock software and saved as a.pdbQT format file. The utilisation of the auto dock vina software facilitates the batch docking of DLGAP5 with small molecule compounds. The configuration file employed for molecular docking must be edited. The following parameters are to be utilised during the docking process: centre_x:-21, centre_y:-2, centre_z:-3, size_x=24, size_y=24, size_z=24. The molecular docking of all ligands and receptors was conducted utilising the Autodock vina command-line batch processing functionality.

*Statistical analysis*

Each experiment was independently repeated on three occasions, and the results were presented as the mean ± standard deviation. $P < 0.05$ indicated a statistically significant difference. All statistical analyses were performed using GraphPad Prism or Image J software. The statistical methods employed in this study include two-tailed unpaired Student's t test, two-tailed paired Student's t test, one-way analysis of variance (ANOVA) and two-way analysis of variance (ANOVA). The specific statistical method applied to each experiment is detailed in the corresponding figure legends.

## Results

*DLGAP5 is highly expressed in tumors and is associated with poor prognosis in SACC*

To identify the potential genes involved in SACC, we analyzed two GEO datasets (GSE88804 and GSE153002). The GSE88804 dataset had 1012 downregulated genes and 806 up-regulated genes, while the GSE153002 dataset had 998 downregulated genes and 901 up-regulated genes (**Figure 1A**, **1B**). We use the Proxy Variable Analysis (SVA) package for batch effect removal and data normalization after data integration. The normalization quality and data distribution were evaluated by drawing box plots before and after normalization and principal component analysis (PCA) (Figure S1A, S1B), and further difference analysis was conducted on the data after batch removal and merging, identifying 975 down-regulated genes

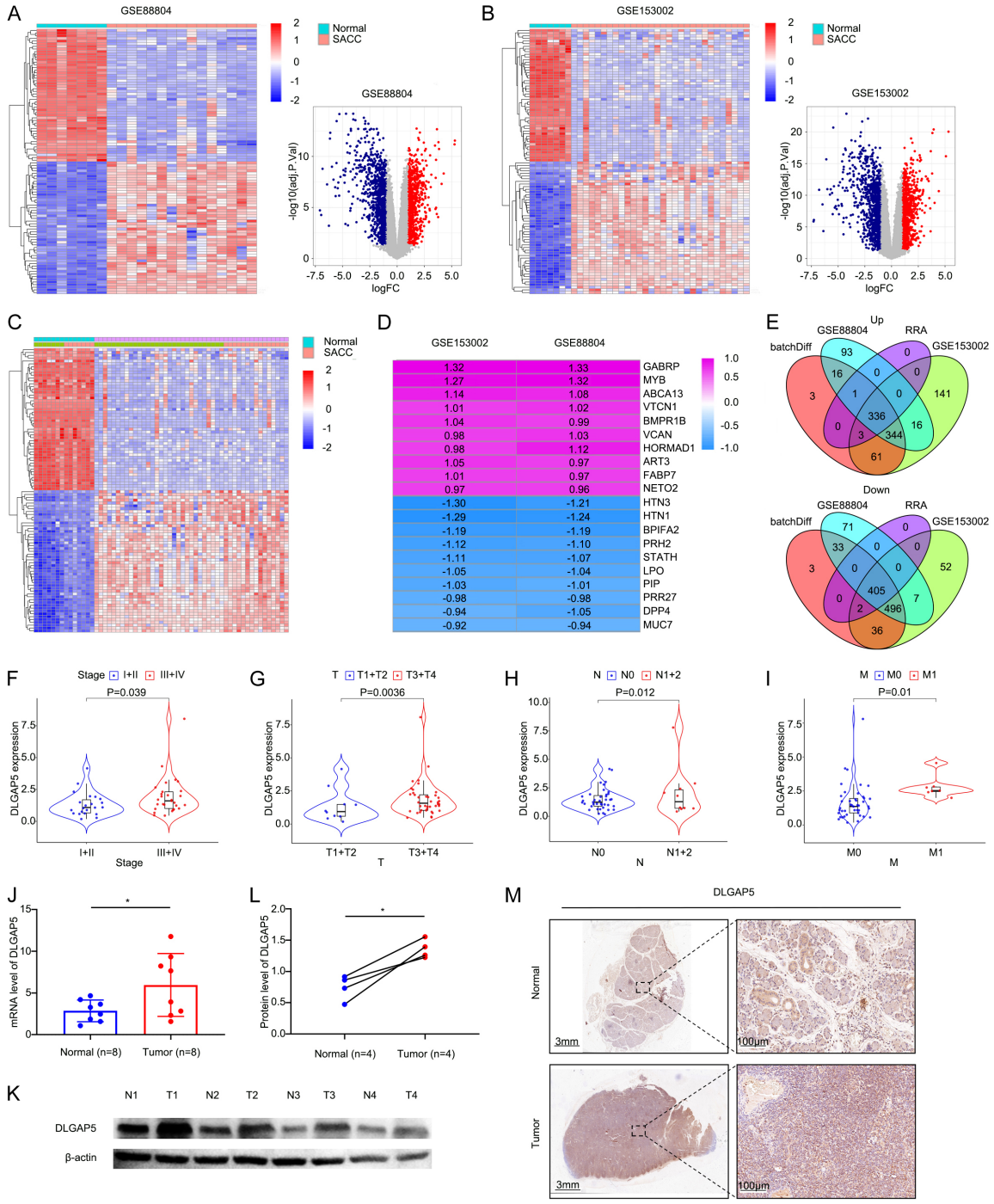


**Figure 1.** DLGAP5 is highly expressed in tumors and is associated with poor prognosis in SACC. A, B: Clustering heat map and volcano plot of GSE88804 and GSE153002. C: Clustering heat map of the data after batch removal and merging. D: The top 20 up-regulated and down-regulated genes of RRA analysis. E: Venn plot to screen the differentially expressed genes. F-I: Analysis of the DLGAP5 expression in SACC with different clinical stage and pathological stage. J: The mRNA expression of DLGAP5 in normal glandular tissues and SACC tissues. K, L: The protein expression of DLGAP5 in paired adjcent normal parotid gland tissues and SACC parotid gland tissues. M: DLGAP5 expression level in normal glandular tissues and SACC tissues using IHC (magnification: 6× and 200×). The data are presented as the means ± SD. *P < 0.05; **P < 0.01; ***P < 0.001 and ****P < 0.0001, Student's t test [F-L].

and 764 up-regulated genes (**Figure 1C**). Our subsequent RRA analysis identified 407 down-regulated genes and 340 up-regulated genes, and presented the top 10 up-regulated

and down-regulated genes (**Figure 1D**). Subsequently, we used the Venn plot to screen the overlapping genes among the differentially expressed genes, and a total of 741 differentially expressed genes were screened out: 336 genes were up-regulated and 405 genes were down-regulated (**Figure 1E**). Then, using the string database, a protein network of DEGs was constructed, and the top twenty proteins were screened out as candidate targets (Figure S1C).

Next, we verified the mRNA expression of the above twenty genes in salivary gland epithelial cells, SACC-83, and SACC-LM. We found that DLGAP5 was lowly expressed in normal salivary gland epithelial cells, but highly expressed in SACC-83 and SACC-LM (Figure S1D).

To further explore the relationship between DLGAP5 and SACC, data form El - Naggar Adel K (https://data.mendeley.com/datasets/6sbv-7bpj5n/1) were analyzed. It was found that the expression level of DLGAP5 in SACC was significantly correlated with the clinical stage (**Figure 1F**), tumor size (**Figure 1G**) and the distant metastasis level (**Figure 1H**, **1I**).

To study the expression of DLGAP5 in SACC tissues, we detected the expression of DLGAP5 in normal glandular tissues and SACC tissues. It was found that the expression of DLGAP5 in SACC increased in both mRNA (**Figure 1J**) and protein (**Figure 1K**, **1L**) levels.

Furthermore, the results of immunohistochemistry showed that the expression of DLGAP5 was significantly higher in SACC than normal salivary gland tissues (**Figure 1M**).

*DLGAP5 facilitates SACC proliferation in vitro and in vivo*

To gain further insight into the impact of DLGAP5, a pan-cancer Gene Set Enrichment Analysis (GSEA) was conducted using the integrated dataset derived from the two GEO datasets (GSE88804 and GSE153002) after batch effect removal. This analysis examined DEGs between NUSAP1-high and -low patients in SACC. The resulting heatmap revealed significant enrichment of cell proliferation-related signaling pathways, including MYC, Mitotic spindle, G2M, and E2F pathways, in the DLGAP5-high patients (**Figure 2A**). This finding aligns with a previous report suggesting that DLGAP5 promotes the organization of mitotic spindle microtubules around chromosomes, indicating its crucial role in regulating cell proliferation [32].

To explore the relationship between DLGAP5 and proliferation, stable DLGAP5 knockdown SACC cell lines were generated, the efficiency of knocking down has been verified by RT-qPCR and western blot assays (**Figure 2B-G**). The role of DLGAP5 in proliferation was examined by CCK-8, colony formation, and EdU staining. These results demonstrated that the knockdown of DLGAP5 resulted in a significant decrease in the capacity of cell proliferation in SACC-83 and SACC-LM cells (**Figure 2H-M**). To determine if DLGAP5 has contributed to the malignant activity of SACC in vivo, we generated subcutaneous tumor nude mouse models. For the subcutaneous tumor model, mice were injected with sh-NC or sh-DLGAP5 SACC-83 cells. The results demonstrated that mice injected with sh-DLGAP5 SACC-83 cells exhibited significantly smaller tumors compared with the control group (**Figure 2N-P**). The subcutaneous tumors were sectioned and assessed with H&E staining and immunohistochemistry for Ki67 expression (**Figure 2Q**, **2R**). Besides, an increase in cell proliferation was observed in SACC-83 and SACC-LM cells in response to the over-expression of DLGAP5 (**Figure 2S-X**). All of the above implies that DLGAP5 may promote SACC cell proliferation both in vitro and in vivo.

*DLGAP5 promotes SACC migration and invasion*

In order to ascertain the effect of DLGAP5 on SACC migration and invasion, a series of experiments were performed, including wound healing and transwell assays. The results demonstrated that downregulating DLGAP5 decreased the capacity of SACC cells for migration and invasion (**Figure 3A-J**). Furthermore, the immunofluorescence assay revealed that the DLGAP5 knockdown group of SACC cells exhibited a reduced expression of the mesenchymal-related protein Vimentin in comparison with the control group (**Figure 3K**). Subsequently, immunohistochemical staining was performed on subcutaneous tumors in nude mice. The results demonstrated that, compared with the control group, the expression level of the mesenchymal-related protein Vimentin was reduced, while the expression level of the epithelial-related protein E-cadherin was increased (**Figure 3L-N**).

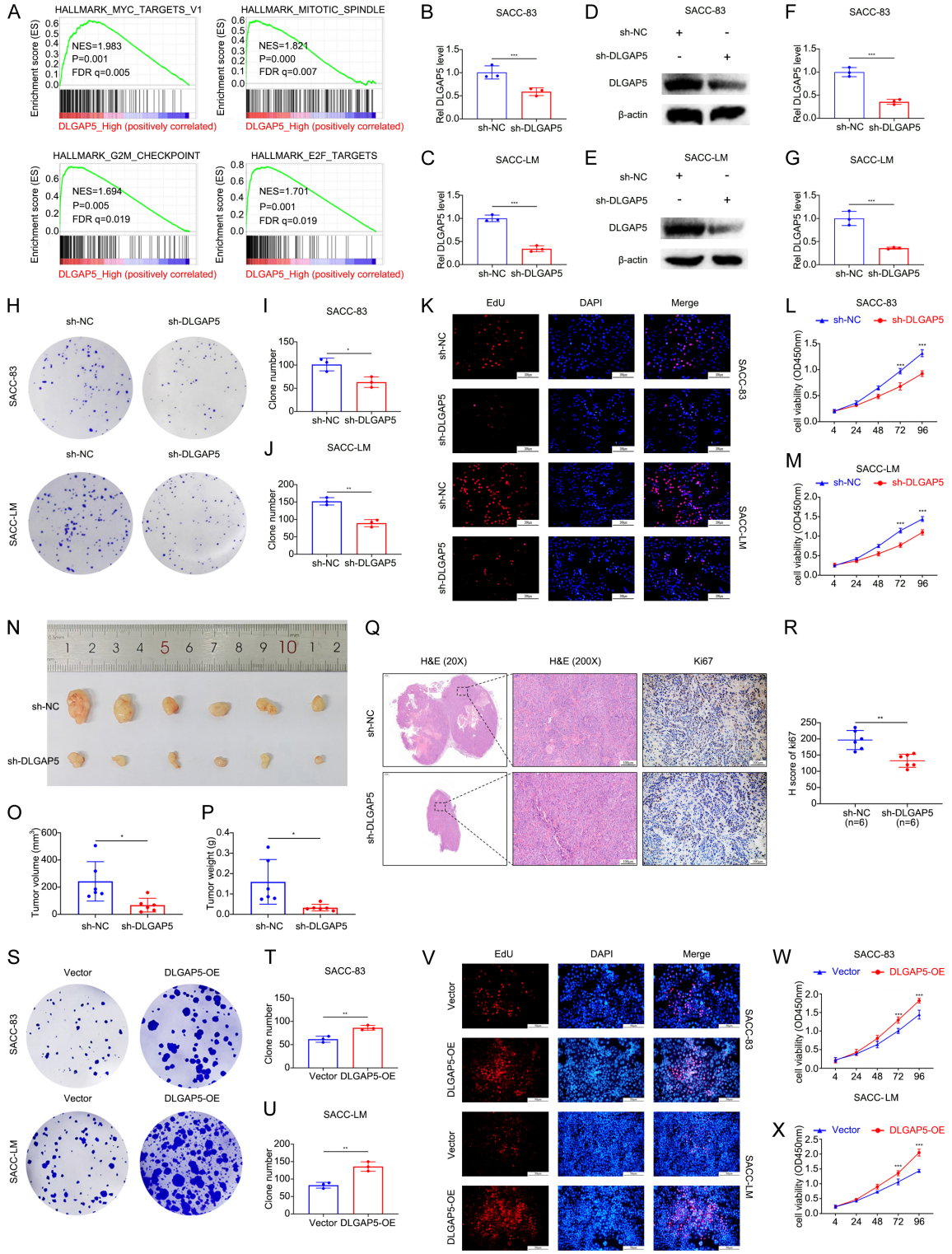


**Figure 2.** DLGAP5 facilitates SACC proliferation in vitro and in vivo. A: GSEA heatmap revealed significant enrichment of MYC, Mitotic spindle, G2M, and E2F pathways. B-G: DLGAP5 knockdown efficiency were evaluated by qRT-PCR and western blot statistical analysis. H-J: Images of representative colonies of the indicated cells and clone number of statistics. K: EdU staining images of DLGAP5 knockdown SACC cells (magnification: 200×). L, M: CCK8 assay to evaluate proliferation of DLGAP5 knockdown SACC cells. N: Subcutaneous tumors of the mice inoculated with the indicated cells. O: Tumor growth curves. P: Tumor weight. Q: H&E staining and IHC detection of Ki-67 expression in subcutaneous tumors (magnification: 20× and 200×). R: IHC score. S-U: Images of representative colonies of the indicated cells and statistical analysis. V: EdU staining images of DLGAP5-overexpressing SACC cells (magnification:

200×). W, X: CCK8 assay to evaluate proliferation of DLGAP5-overexpressing SACC cells. The data are presented as the means ± SD. *P < 0.05; **P < 0.01; ***P < 0.001 and ****P < 0.0001, Student's t test [B, C, F, G, I, J, O, P, R, T and U], two-way repeated measures ANOVA [L, M, W, and X].

In addition, the upregulation of DLGAP5 could also promote the migration and invasion abilities of SACC cells (**Figure 3O-X**).

*DLGAP5 promotes SACC progression through PI3K/AKT signaling pathway*

In order to gain further insight into the molecular mechanism by which DLGAP5 exerts its oncogenic effects in SACC, we conducted RNA-seq to discern the DEGs between sh-NC and sh-DLGAP5 SACC-LM cells (**Figure 4A**). KEGG enrichment analysis revealed that the PI3K/AKT pathway linked to cell proliferation significantly activated (**Figure 4B**). Therefore, we further investigated whether the effects of DLGAP5 were dependent on PI3K/AKT signaling. As demonstrated in **Figure 4C**, the levels of PI3K, AKT, and phospho-AKT proteins were reduced following the knockdown of DLGAP5. These results suggest that DLGAP5 might activate the PI3K/AKT pathway in tumor progression. To investigate this hypothesis, DLGAP5-overexpressed SACC-83 and SACC-LM cells were treated with PI3K inhibitor (LY294002). The colony formation and CCK8 assays demonstrated that the proliferation of DLGAP5-overexpressed cells was significantly suppressed with the treatment of LY294002 (**Figure 4D-F**). Furthermore, the results of the wound healing and transwell assays demonstrated that the migration and invasion abilities of the DLGAP5-overexpressing cells were significantly inhibited by the treatment with LY294002 (**Figure 4G-M**). These observations indicate that DLGAP5 exerts a regulatory effect on the proliferation and the process of EMT of SACC cells by activating the PI3K/AKT pathway.

*ZINC3809191 targets DLGAP5 to suppress tumor progression*

To identify the lead compounds that target DLGAP5 and inhibit cancer progression, we performed virtual screen in world database, approved drugs in major juridications, including the FDA, i.e DrugBank approved (https://zinc15.docking.org/substances/subsets/world/) (**Figure 5A**). The three-dimensional structure of DLGAP5 was modeled using AlphaFold3. Through structure-based virtual screening targeting the DLGAP5 protein, five candidate compounds exhibiting high binding affinity were selected for functional evaluation (**Figure 5B**). Compared with other compounds, ZINC3809191 was found to exert a most significantly inhibitory effect on SACC cell proliferation (**Figure 5C**, **5D**). Furthermore, we detected the effect of ZINC3809191 on the proliferation ability of SACC cells through colony formation experiments. The results indicated that ZINC3809191 could significantly inhibit the colony formation ability of SACC cells (**Figure 5E**). Furthermore, molecular docking and dynamics simulations suggested that Ser533, Asn538 in DLGAP5 may be responsible for its binding with ZINC3809191 (**Figure 5F**). Besides, our transwell assays and wound healing assays results found that the ZINC3809191 can also inhibit the EMT procession (**Figure 5G-J**).

In order to explore the role of ZINC3809191 in vivo, subcutaneous tumour was conducted in nude mice using SAC-83 cells and SAC-LM cells, and ZINC3809191 was injected. The results demonstrate that ZINC3809191 has the capacity to inhibit tumour growth to a significant degree (**Figure 5K-O**). Taken together, we have identified a potential targeted inhibitor of DLGAP5 that can promote tumor growth and metastasis.

## Discussion

SACC, the second most prevalent malignant neoplasm of the salivary gland, exhibits a slow natural progression [33, 34]. However, the disease is distinguished by its high recurrence rate [35], perineuronal infiltration [36], and distant metastasis [37], particularly in the lung [38]. Consequently, the overall prognosis of SACC remains poor, with the long-term overall survival rate ranging from 23% to 40% [39]. In this study, we revealed the key role of DLGAP5 in the occurrence and development of SACC. In order to ascertain the potential genes associated with SACC, a comprehensive analysis of two GEO datasets (GSE88804 and GSE153002) was conducted. Subsequent to the elimination of batch effects and the integration of data, a further difference analysis was con-

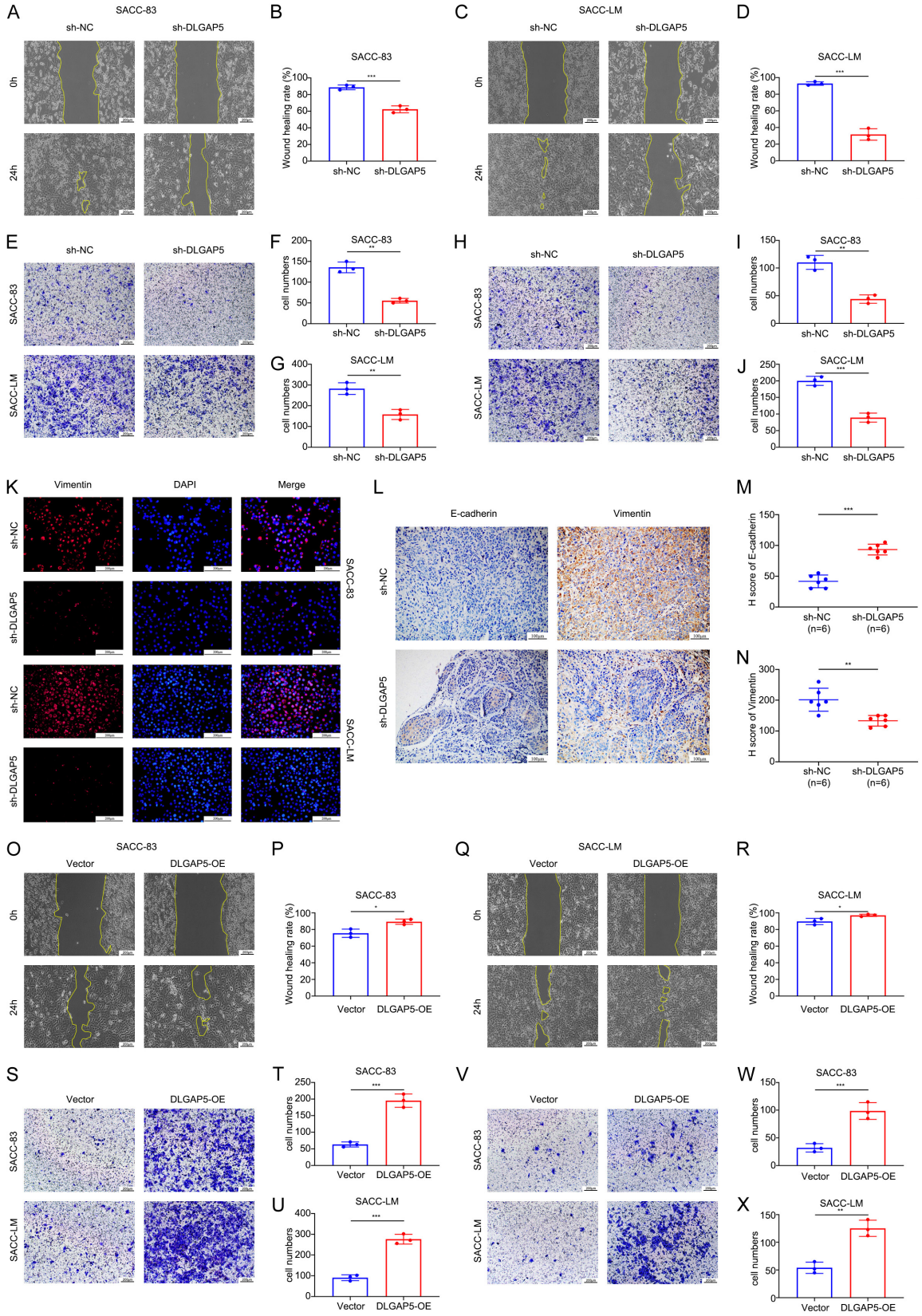


**Figure 3.** DLGAP5 promotes SACC migration and invasion. A, B: The migration ability was evaluated in SACC-83 cells with DLGAP5 knockdown using wound healing assay and its statistical analysis (magnification: 100×). C, D: The

migration ability was evaluated in SACC-LM cells with DLGAP5 knockdown using wound healing assay and its statistical analysis (magnification: 100×). E-G: Transwell assay to assess the migration ability of SACC-83 and SACC-LM cells with DLGAP5 knockdown and its statistical analysis (magnification: 100×). H-J: Invasion ability of SACC-83 and SACC-LM cells with DLGAP5 knockdown and its statistical analysis (magnification: 100×). K: Immunofluorescence assay to determine the Vimentin in SACC cells (magnification: 200×). L-N: IHC detection of E-cadherin and Vimentin expression in subcutaneous tumors and IHC score (magnification: 200×). O-R: The migration ability of SACC-83 and SACC-LM cells with overexpression of DLGAP5 was evaluated by wound healing experiments and statistical analysis (magnification: 100×). S-X: The migration and invasion abilities of SACC-83 and SACC-LM cells with overexpression of DLGAP5 were evaluated by the transwell assays and statistical analysis was conducted (magnification: 100×). The data are presented as the means ± SD. *P < 0.05; **P < 0.01; ***P < 0.001 and ****P < 0.0001, Student's t test [B, D, F, G, I, J, M, N, P, R, T, U, W and X].

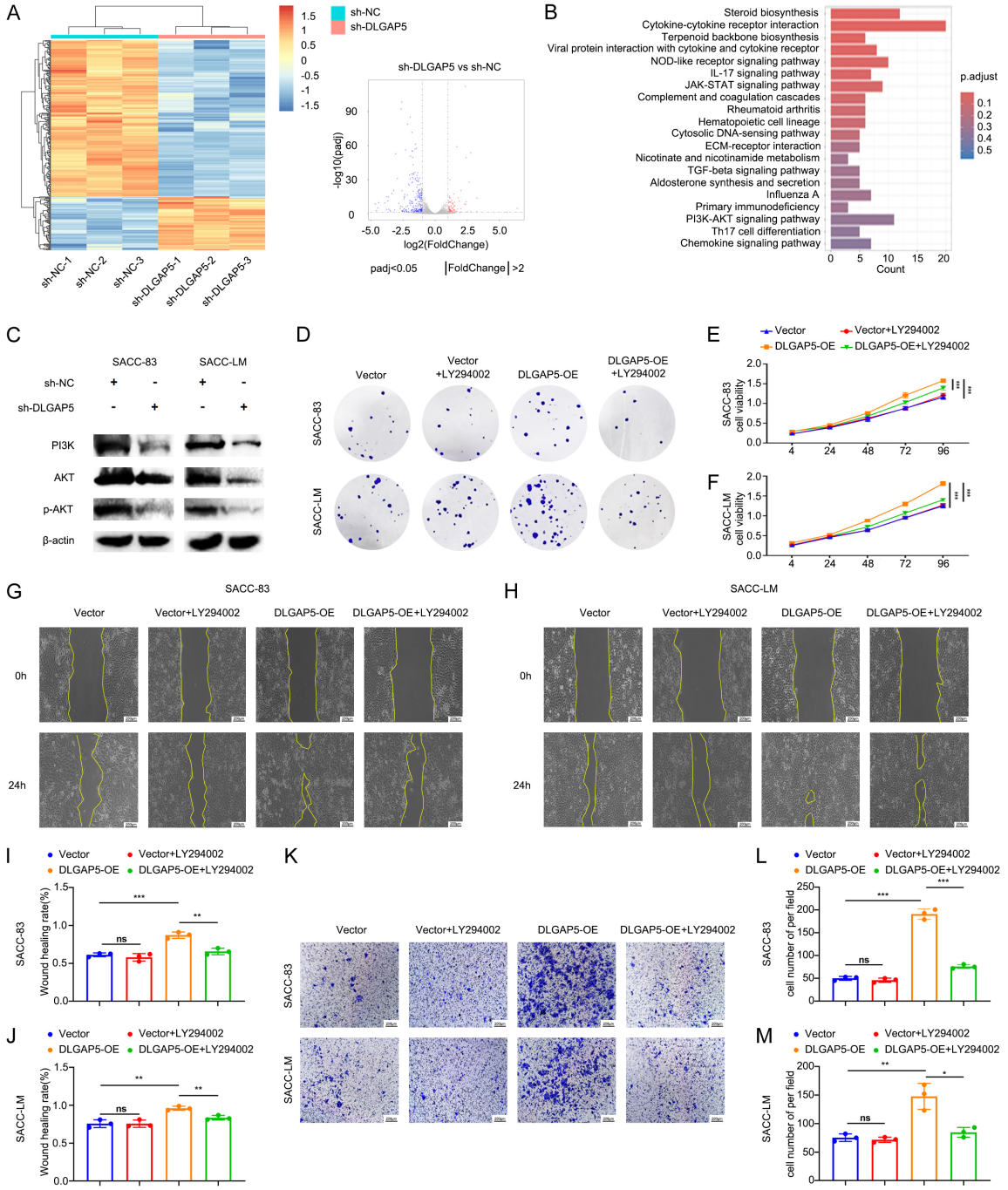

**Figure 4.** DLGAP5 promotes SACC progression through the PI3K/AKT signaling pathway. A: Clustering heat map and volcano map of the RNA-seq data between sh-NC and sh-DLGAP5 cells. B: KEGG pathway analysis of the RNA-seq data. C: Western blot analysis of PI3K/AKT pathway-related protein expression in SACC cells. D: Images of representative colonies of the SACC cells treated with LY294002. E, F: CCK8 assay to evaluate DLGAP5-OE cells treated with LY294002. G-J: The migration ability of SACC cells treated with LY294002 was measured with wound healing assay and statistical analysis (magnification: 100×). K-M: Transwell assay to assess SACC-83 and SACC-LM cells treated with LY294002 (magnification: 100×). The data are presented as the means ± SD. *P < 0.05; **P < 0.01; ***P < 0.001 and ****P < 0.0001, two-way repeated measures ANOVA [E, F], one-way ANOVA [I, J, L and M].

ducted on the data. Subsequent bioinformatics analysis and RT-qPCR verification identified that DLGAP5 is significantly overexpressed in SACC.

The DLGAP family, which consists of five members (DLGAP1-5), was first discovered in rats and has three key domains [40]. The protein contains a 14-amino acid repeating domain, a dynamic protein light chain domain, and a guanosine kinase-associated protein homologous domain [41, 42]. According to the extant literature, DLGAP5 has been implicated in the development and progression of various neoplasias, including bladder cancer [43], endometrial cancer [19], ovarian cancer [14] and lung cancer [44, 45]. In this study, we systematically investigated the clinical revelance of DLGAP5 in SACC. Notably, DLGAP5 expression levels exhibited strong positive correlations with advanced clinical stages and higher pathological grades. These findings indicated that DLGAP5 may act as a prognostic biomarker and an effective target for SACC therapy.

To investigate the function of DLGAP5 in the biological process of SACC, two DLGAP5-knockdown and two DLGAP5-overexpressed SACC cell lines were established. Cytological experiments have demonstrated that the knockdown of DLGAP5 can significantly inhibit the proliferation, migration, and invasion of SACC in vitro. Conversely, the overexpressed of DLGAP5 has been observed to significantly promote the proliferation, migration, and invasion of SACC. In addition, subcutaneous tumor model was established in mice by subcutaneous injection of SACC-83-sh-NC and SACC-83-sh-DLGAP5 cells. The results indicated that the knockdown of DLGAP5 could inhibit the growth of SACC in vivo, consistent with the results in vitro.

In order to investigate the specific mechanism of DLGAP5 in SACC, RNA-seq was conducted on SACC-LM-sh-NC and SACC-LM-sh-DLGAP5 cells. The results indicated that the pro-cancer effect of DLGAP5 was mediated by the PI3K/AKT signal. It is widely known that the PI3K/AKT pathway plays a critical role in the development of malignant tumors and is a significant mechanism contributing to tumorigenesis [46, 47]. In this study, we demonstrated that the knockdown of DLGAP5 resulted in the inhibition of the PI3K/AKT pathway. Subsequent experimental investigations revealed that the PI3K inhibitor (LY294002) was capable of reversing the alterations in proliferation, migration, and invasion capacity induced by the over-expression of DLGAP5. This finding suggests that the activation of the DLGAP5/PI3K/AKT pathway plays a substantial role in the development and progression of SACC.

In order to explore the potential targeted therapy of DLGAP5, five potential inhibitors were screened out through virtual screening. Among these, the compound ZINC3809191 demonstrated the strongest tumor suppression ability. Molecular docking and dynamic simulations suggested that Ser533 and Asn538 in DLGAP5 might be responsible for its binding with ZINC3809191. Vitro experiments further demonstrated that ZINC3809191 could inhibit the proliferation, migration, and invasion abilities of SACC cells. These findings not only reveal the feasibility of DLGAP5 as a drug target, but also provide a lead compound with therapeutic potential, ZINC3809191, which has significant anti-tumor activity targeting DLGAP5, offering an important theoretical basis for the drug development of this disease.

In conclusion, DLGAP5 is upregulated in SACC and is associated with clinical stage and pathological grade, playing a regulatory role in cell proliferation, migration, and invasion. Additionally, the identification of ZINC3809191 with significant anti-tumor activity against DLGAP5 provides a crucial theoretical foundation for the potential therapeutic strategies for SACC.

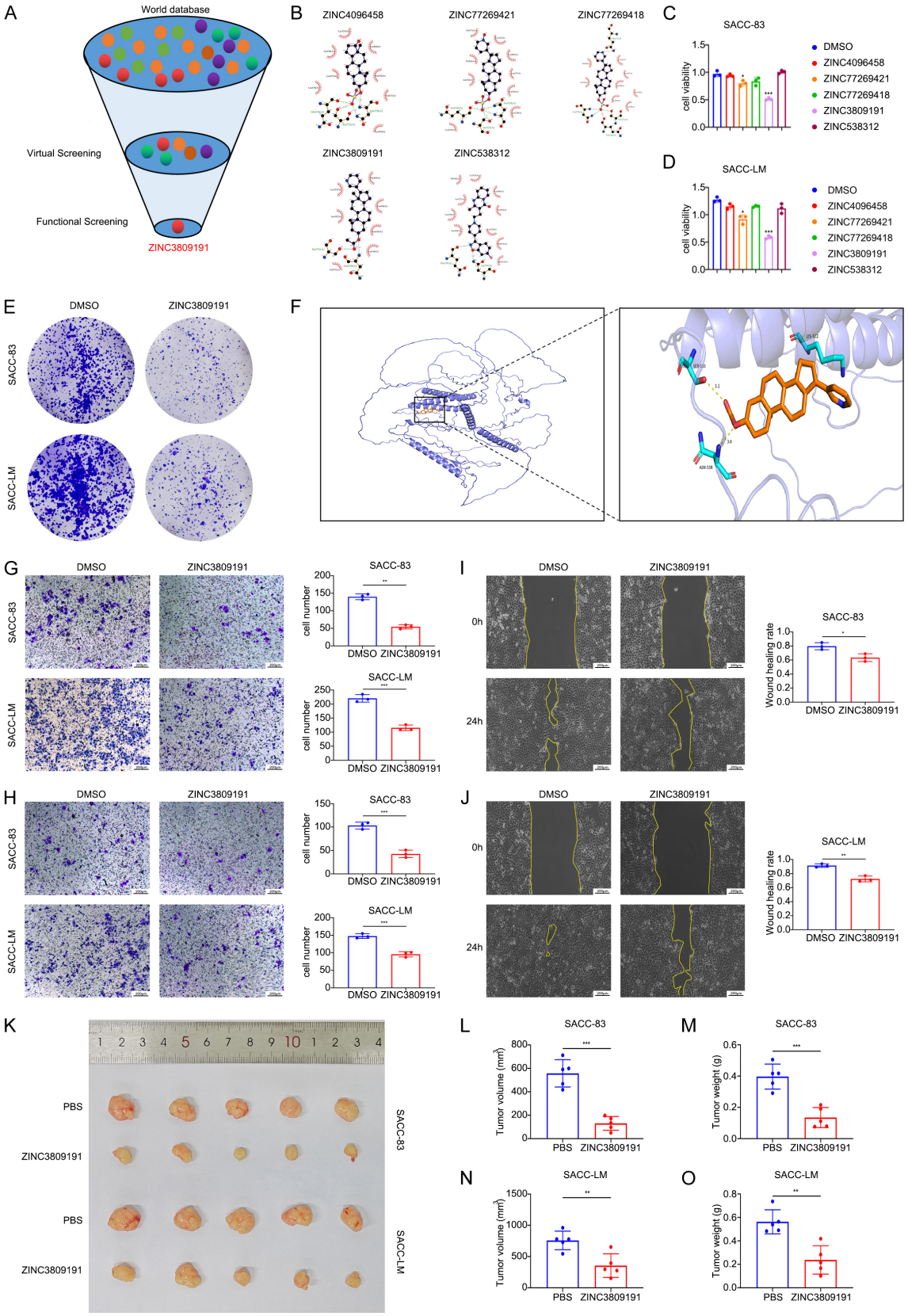


**Figure 5.** ZINC3809191 targets DLGAP5 to suppress tumor progression. A: Schematic diagram of screening strategies for the DLGAP5-targeting small molecule compounds. B: The docking conformation of DLGAP5 with the top 5

small molecule compounds in terms of binding energy and its interaction forces with key residues. C, D: The inhibitory effects of 5 candidate compounds on SACC cell proliferation were detected with CCK8 assay. E: Images of representative colonies of the indicated cells. F: The structure of the DLGAP5 protein complexed with ZINC3809191. G, H: Transwell assay to assess the migration and invasion ability of SACC-83 and SACC-LM cells treated with ZINC3809191 (magnification: 100×). I, J: Wound healing assay and its statistical analysis of SACC cells treated with ZINC3809191 (magnification: 100×). K: Subcutaneous tumors of the mice injected with PBS or ZINC3809191. L, M: Tumor growth curves and tumor weight of SACC-83. N, O: Tumor growth curves and tumor weight of SACC-LM. The data are presented as the means ± SD. *P < 0.05; **P < 0.01; ***P < 0.001 and ****P < 0.0001, one-way ANOVA [C and D], Student's t test [G-J, L-O].

## Acknowledgements

This work was supported by the Technology Innovation Platform at Zhongnan Hospital of Wuhan University (PTXM2024002).

Informed consents were obtained from the patients.

## Disclosure of conflict of interest

None.

**Address correspondence to:** Xiu-Hong Weng and Bo Cheng, Department of Stomatology, Zhongnan Hospital of Wuhan University, No. 169 Donghu Road, Wuhan 430071, Hubei, China. E-mail: ZN003825@whu.edu.cn (XHW); chengbo@znhospital.cn (BC)

## References

[1] Seok J, Lee DY, Kim WS, Jeong WJ, Chung EJ, Jung YH, Kwon SK, Kwon TK, Sung MW and Ahn SH. Lung metastasis in adenoid cystic carcinoma of the head and neck. Head Neck 2019; 41: 3976-83.

[2] Coca-Pelaz A, Rodrigo JP, Bradley PJ, Vander Poorten V, Triantafyllou A, Hunt JL, Strojan P, Rinaldo A, Haigentz M Jr, Takes RP, Mondin V, Teymoortash A, Thompson LD and Ferlito A. Adenoid cystic carcinoma of the head and neck - an update. Oral Oncol 2015; 51: 652-61.

[3] Emerick C, Mariano FV, Vargas PA, Nör JE, Squarize CH and Castilho RM. Adenoid cystic carcinoma from the salivary and lacrimal glands and the breast: different clinical outcomes to the same tumor. Crit Rev Oncol Hematol 2022; 179: 103792.

[4] He S, Li P, Zhong Q, Hou L, Yu Z, Huang Z, Chen X, Fang J and Chen X. Clinicopathologic and prognostic factors in adenoid cystic carcinoma of head and neck minor salivary glands: a clinical analysis of 130 cases. Am J Otolaryngol 2017; 38: 157-62.

[5] Nascimento de Aquino S, Silvestre Verner F, Álvares Cabral R, Najar Rios CH, Paes de Almeida O and Sánchez-Romero C. Adenoid cystic carcinoma with myoepithelial predominance affecting maxilla and maxillary sinus. J Stomatol Oral Maxillofac Surg 2019; 120: 55-60.

[6] Bell D, Bell AH, Bondaruk J, Hanna EY and Weber RS. In-depth characterization of the salivary adenoid cystic carcinoma transcriptome with emphasis on dominant cell type. Cancer 2016; 122: 1513-22.

[7] Moskaluk CA. Adenoid cystic carcinoma: clinical and molecular features. Head Neck Pathol 2013; 7: 17-22.

[8] van der Wal JE, Becking AG, Snow GB and van der Waal I. Distant metastases of adenoid cystic carcinoma of the salivary glands and the value of diagnostic examinations during follow-up. Head Neck 2002; 24: 779-83.

[9] Tchekmedyian V, Sherman EJ, Dunn L, Tran C, Baxi S, Katabi N, Antonescu CR, Ostrovnaya I, Haque SS, Pfister DG and Ho AL. Phase II study of lenvatinib in patients with progressive, recurrent or metastatic adenoid cystic carcinoma. J Clin Oncol 2019; 37: 1529-37.

[10] da Silva FJ, Carvalho de Azevedo J Jr, Ralph ACL, Pinheiro JJV, Freitas VM and Calcagno DQ. Salivary glands adenoid cystic carcinoma: a molecular profile update and potential implications. Front Oncol 2023; 13: 1191218.

[11] Nomura N, Miyajima N, Sazuka T, Tanaka A, Kawarabayasi Y, Sato S, Nagase T, Seki N, Ishikawa K and Tabata S. Prediction of the coding sequences of unidentified human genes. I. The coding sequences of 40 new genes (KIAA0001-KIAA0040) deduced by analysis of randomly sampled cDNA clones from human immature myeloid cell line KG-1. DNA Res 1994; 1: 27-35.

[12] Deng Y, Li H, Song Y, Cen J, Zhang Y, Sui Y, Cui D, Li TC, Xu Y, Wang CC, Chung PWJ and Tang T. Whole genome transcriptomic analysis of ovary granulosa cells revealed an anti-apoptosis regulatory gene DLGAP5 in polycystic ovary syndrome. Front Endocrinol (Lausanne) 2022; 13: 781149.

[13] Tsou AP, Yang CW, Huang CY, Yu RC, Lee YC, Chang CW, Chen BR, Chung YF, Fann MJ, Chi CW, Chiu JH and Chou CK. Identification of a novel cell cycle regulated gene, HURP, overexpressed in human hepatocellular carcinoma. Oncogene 2003; 22: 298-307.

[14] Li W, Lin J, Huang J, Chen Z, Sheng Q, Yang F, Yang X and Cui X. MicroRNA-409-5p inhibits cell proliferation, and induces G2/M phase arrest and apoptosis by targeting DLGAP5 in ovarian cancer cells. Oncol Lett 2022; 24: 261.
[15] Zhang H, Liu Y, Tang S, Qin X, Li L, Zhou J, Zhang J and Liu B. Knockdown of DLGAP5 suppresses cell proliferation, induces G2/M phase arrest and apoptosis in ovarian cancer. Exp Ther Med 2021; 22: 1245.
[16] Liao W, Liu W, Yuan Q, Liu X, Ou Y, He S, Yuan S, Qin L, Chen Q, Nong K, Mei M and Huang J. Silencing of DLGAP5 by siRNA significantly inhibits the proliferation and invasion of hepatocellular carcinoma cells. PLoS One 2013; 8: e80789.
[17] Zhang Q, Wang Y and Xue F. ASPM, CDC20, DLGAP5, BUB1B, CDCA8, and NCAPG may serve as diagnostic and prognostic biomarkers in endometrial carcinoma. Genet Res (Camb) 2022; 2022: 3217248.
[18] Zheng R, Shi Z, Li W, Yu J, Wang Y and Zhou Q. Identification and prognostic value of DLGAP5 in endometrial cancer. PeerJ 2020; 8: e10433.
[19] Chen R, Liu J, Hu J, Li C, Liu Y and Pan W. DLGAP5 knockdown inactivates the Wnt/β-catenin signal to repress endometrial cancer cell malignant activities. Environ Toxicol 2023; 38: 685-93.
[20] Schneider MA, Christopoulos P, Muley T, Warth A, Klingmueller U, Thomas M, Herth FJ, Dienemann H, Mueller NS, Theis F and Meister M. AURKA, DLGAP5, TPX2, KIF11 and CKAP5: five specific mitosis-associated genes correlate with poor prognosis for non-small cell lung cancer patients. Int J Oncol 2017; 50: 365-72.
[21] Chen M, Zhang S, Wang F, He J, Jiang W and Zhang L. DLGAP5 promotes lung adenocarcinoma growth via upregulating PLK1 and serves as a therapeutic target. J Transl Med 2024; 22: 209.
[22] Shi YX, Yin JY, Shen Y, Zhang W, Zhou HH and Liu ZQ. Genome-scale analysis identifies NEK2, DLGAP5 and ECT2 as promising diagnostic and prognostic biomarkers in human lung cancer. Sci Rep 2017; 7: 8072.
[23] Li Y, Wei J, Sun Y, Zhou W, Ma X, Guo J, Zhang H and Jin T. DLGAP5 regulates the proliferation, migration, invasion, and cell cycle of breast cancer cells via the JAK2/STAT3 signaling axis. Int J Mol Sci 2023; 24: 15819.
[24] Wang Y, Kang J, Wang R, Ramezani K, Bonakdar M, Moghimi N, Salimi M, Yao Y and Wang K. Bisphenol A interacts with DLGAP5 and regulates IL-6/JAK2/STAT3 signaling pathway to promote tumorigenesis and progression of osteosarcoma. Chemosphere 2023; 312: 136545.
[25] Huang J, Zheng M, Li Y, Xu D and Tian D. DLGAP5 promotes gallbladder cancer migration and tumor-associated macrophage M2 polarization by activating cAMP. Cancer Immunol Immunother 2023; 72: 3203-16.
[26] Zhou F, Deng Z, Shen D, Lu M, Li M, Yu J, Xiao Y, Wang G, Qian K, Ju L and Wang X. DLGAP5 triggers proliferation and metastasis of bladder cancer by stabilizing E2F1 via USP11. Oncogene 2024; 43: 594-607.
[27] Ballante F, Kooistra AJ, Kampen S, de Graaf C and Carlsson J. Structure-based virtual screening for ligands of G protein-coupled receptors: what can molecular docking do for you? Pharmacol Rev 2021; 73: 527-565.
[28] Carlsson J and Luttens A. Structure-based virtual screening of vast chemical space as a starting point for drug discovery. Curr Opin Struct Biol 2024; 87: 102829.
[29] Gorgulla C. Recent developments in ultralarge and structure-based virtual screening approaches. Annu Rev Biomed Data Sci 2023; 6: 229-58.
[30] Soldi R, Ghosh Halder T, Weston A, Thode T, Drenner K, Lewis R, Kaadige MR, Srivastava S, Daniel Ampanattu S, Rodriguez del Villar R, Lang J, Vankayalapati H, Weissman B, Trent JM, Hendricks WPD and Sharma S. The novel reversible LSD1 inhibitor SP-2577 promotes anti-tumor immunity in SWItch/Sucrose-NonFermentable (SWI/SNF) complex mutated ovarian cancer. PLoS One 2020; 15: e0235705.
[31] Noce B, Di Bello E, Fioravanti R and Mai A. LSD1 inhibitors for cancer treatment: focus on multi-target agents and compounds in clinical trials. Front Pharmacol 2023; 14: 1120911.
[32] Wang G, Li M and Zou P. Enzyme-mediated proximity labeling reveals the co-translational targeting of DLGAP5 mRNA to the centrosome during mitosis. RSC Chem Biol 2025; 6: 919-932.
[33] Ho AS, Ochoa A, Jayakumaran G, Zehir A, Valero Mayor C, Tepe J, Makarov V, Dalin MG, He J, Bailey M, Montesion M, Ross JS, Miller VA, Chan L, Ganly I, Dogan S, Katabi N, Tsipouras P, Ha P, Agrawal N, Solit DB, Futreal PA, El Naggar AK, Reis-Filho JS, Weigelt B, Ho AL, Schultz N, Chan TA and Morris LG. Genetic hallmarks of recurrent/metastatic adenoid cystic carcinoma. J Clin Invest 2019; 129: 4276-89.
[34] Ciccolallo L, Licitra L, Cantú G and Gatta G; EUROCARE Working Group. Survival from salivary glands adenoid cystic carcinoma in European populations. Oral Oncol 2009; 45: 669-74.
[35] Lee SM, Jang BS, Park W, Kim YB, Song JH, Kim JH, Kim TH, Kim IA, Lee JH, Ahn SJ, Kim K, Chang AR, Kwon J, Park HJ and Shin KH. Locoregional recurrence in adenoid cystic carci-

noma of the breast: a retrospective, multicenter study (KROG 22-14). Cancer Res Treat 2025; 57: 150-8.
[36] Guazzo E and Panizza B. Management of advanced adenoid cystic carcinoma infiltrating the skull base: a contemporary review. J Neurooncol 2020; 150: 419-27.
[37] Liu S, Yang J, Lu H, Wu Y, Yang W, Xu W and Zhang C. Adenoid cystic carcinoma of submandibular gland: emphasis on locoregional metastasis and prognosis. Oral Dis 2024; 30: 1152-62.
[38] Kong J, Tian H, Zhang F, Zhang Z, Li J, Liu X, Li X, Liu J, Li X, Jin D, Yang X, Sun B, Guo T, Luo Y, Lu Y, Lin B and Liu T. Extracellular vesicles of carcinoma-associated fibroblasts creates a pre-metastatic niche in the lung through activating fibroblasts. Mol Cancer 2019; 18: 175.
[39] Xu B, Drill E, Ho A, Ho A, Dunn L, Prieto-Granada CN, Chan T, Ganly I, Ghossein R and Katabi N. Predictors of outcome in adenoid cystic carcinoma of salivary glands: a clinicopathologic study with correlation between MYB fusion and protein expression. Am J Surg Pathol 2017; 41: 1422-32.
[40] Sabio G, Arthur JS, Kuma Y, Peggie M, Carr J, Murray-Tait V, Centeno F, Goedert M, Morrice NA and Cuenda A. p38γ regulates the localisation of SAP97 in the cytoskeleton by modulating its interaction with GKAP. EMBO J 2005; 24: 1134-45.
[41] Naisbitt S, Valtschanoff J, Allison DW, Sala C, Kim E, Craig AM, Weinberg RJ and Sheng M. Interaction of the postsynaptic density-95/guanylate kinase domain-associated protein complex with a light chain of myosin-V and dynein. J Neurosci 2000; 12: 4524-34.
[42] Tong J, Yang H, Eom SH, Chun C and Im YJ. Structure of the GH1 domain of guanylate kinase-associated protein from Rattus norvegicus. Biochem Biophys Res Commun 2014; 452: 130-5.
[43] Rao X, Cao H, Yu Q, Ou X, Deng R and Huang J. NEAT1/MALAT1/XIST/PKD--Hsa-Mir-101-3p--DLGAP5 axis as a novel diagnostic and prognostic biomarker associated with immune cell infiltration in bladder cancer. Front Genet 2022; 13: 892535.
[44] Shi S, Wu T, Ma Z, Zhang X, Xu K, Tian Q, Gao L, Yin X, Xu S and Yang S. Serum-derived extracellular vesicles promote the growth and metastasis of non-small cell lung cancer by delivering the m6A methylation regulator HNRNPC through the regulation of DLGAP5. J Cancer Res Clin Oncol 2023; 149: 4639-51.
[45] Tang X, Zhou H and Liu Y. High expression of DLGAP5 indicates poor prognosis and immunotherapy in lung adenocarcinoma and promotes proliferation through regulation of the cell cycle. Dis Markers 2023; 2023: 9292536.
[46] Bai M, Che Y, Lu K and Fu L. Analysis of deubiquitinase OTUD5 as a biomarker and therapeutic target for cervical cancer by bioinformatic analysis. PeerJ 2020; 8: e9146.
[47] Han Y, Chen M, Wang A and Fan X. STAT3-induced upregulation of lncRNA CASC11 promotes the cell migration, invasion and epithelial-mesenchymal transition in hepatocellular carcinoma by epigenetically silencing PTEN and activating PI3K/AKT signaling pathway. Biochem Biophys Res Commun 2019; 508: 472-9.

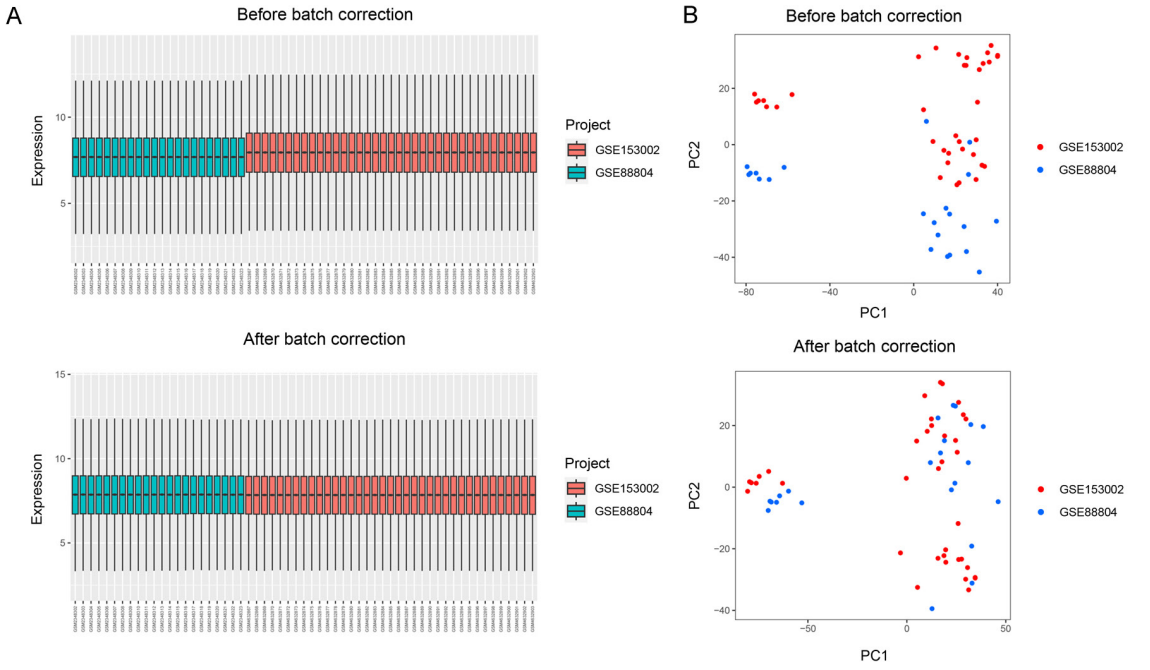
A
Before batch correction
Expression
Project
GSE153002
GSE88804
After batch correction
B
Before batch correction
PC2
PC1
GSE153002
GSE88804
After batch correction

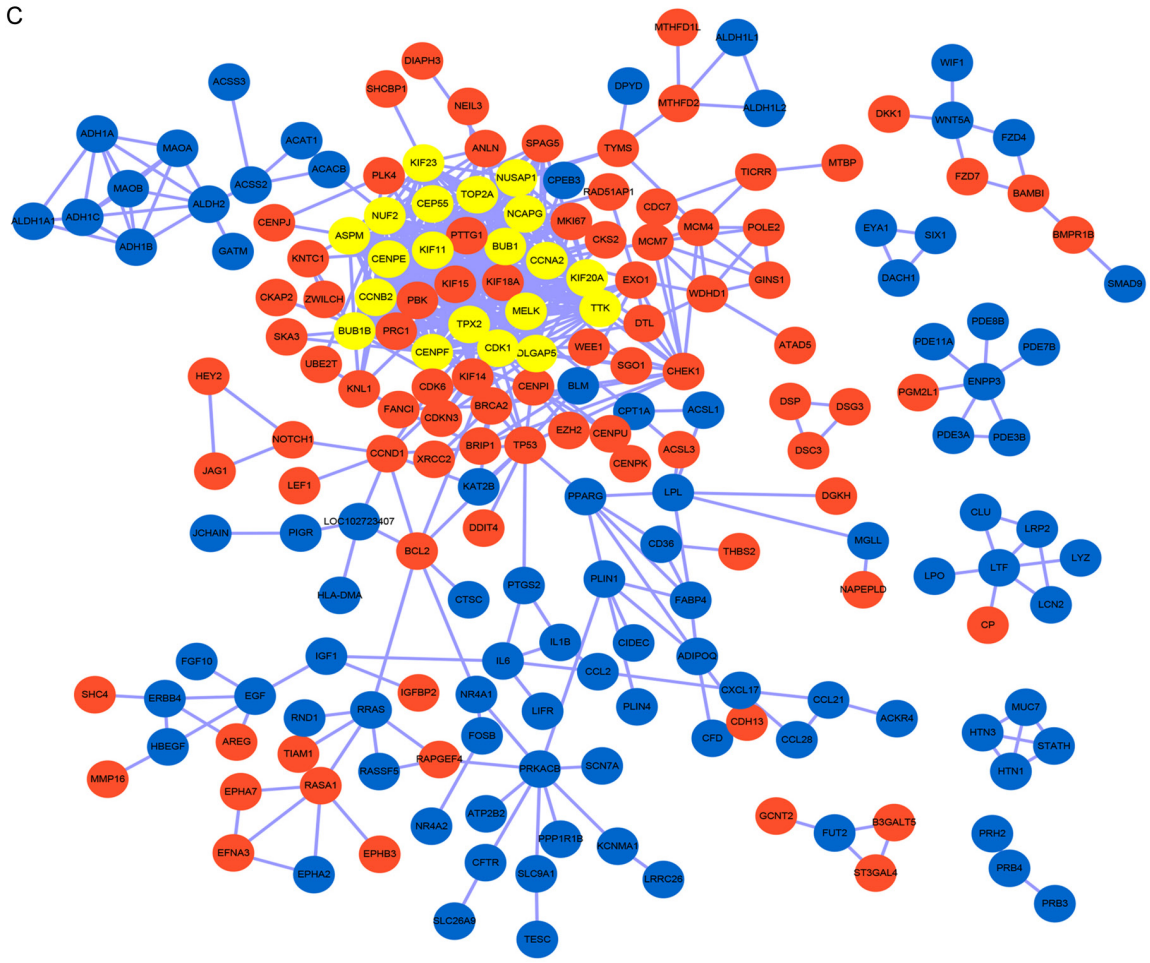
C
MTHFD1L
ALDH1L1
DIAPH3
SHCBP1
NEIL3
DPYD
MTHFD2
ALDH1L2
ACSS3
ADH1A
MAOA
ACAT1
ANLN
SPAG5
TYMS
KIF23
ACACB
PLK4
NUSAP1
CPEB3
TICRR
MTBP
MAOB
ACSS2
ALDH2
TOP2A
RAD51AP1
CDC7
ALDH1A1
ADH1C
CENPJ
NUF2
CEP55
NCAPG
MKI67
MCM4
POLE2
ASPM
PTTG1
CKS2
MCM7
ADH1B
GATM
KNTC1
CENPE
KIF11
BUB1
CCNA2
GINS1
CKAP2
ZWILCH
CCNB2
PBK
KIF15
KIF18A
KIF20A
EXO1
WDHD1
SKA3
BUB1B
PRC1
TPX2
MELK
TTK
DTL
ATAD5
UBE2T
CENPF
CDK1
OLGAP5
WEE1
SGO1
CHEK1
HEY2
KNL1
CDK6
KIF14
CENPI
BLM
FANCI
CDKN3
BRCA2
CPT1A
ACSL1
NOTCH1
CCND1
XRCC2
BRIP1
TP53
EZH2
CENPU
ACSL3
JAG1
LEF1
CENPK
KAT2B
PPARG
LPL
DGKH
JCHAIN
PIGR
LOC102723407
DDIT4
CD36
THBS2
MGLL
BCL2
HLA-DMA
CTSC
PTGS2
PLIN1
FABP4
NAPEPLD
CIDEC
ADIPOQ
IL1B
IL6
CCL2
IGF1
FGF10
SHC4
ERBB4
EGF
IGFBP2
NR4A1
CXCL17
CCL21
ACKR4
RND1
RRAS
LIFR
PLIN4
CDH13
CFD
CCL28
HBEGF
AREG
TIAM1
FOSB
RAPGEF4
MMP16
RASSF5
PRKACB
SCN7A
EPHA7
RASA1
NR4A2
ATP2B2
EFNA3
EPHB3
EPHA2
CFTR
PPP1R12B
KCNMA1
SLC9A1
LRRC26
SLC26A9
TESC
WIF1
DKK1
WNT5A
FZD4
FZD7
BAMBI
EYA1
SIX1
BMPR1B
DACH1
SMAD9
PDE8B
PDE11A
PDE7B
PGM2L1
ENPP3
PDE3A
PDE3B
DSP
DSG3
DSC3
CLU
LRP2
LYZ
LPO
LTF
LCN2
CP
MUC7
HTN3
STATH
HTN1
GCNT2
FUT2
B3GALT5
ST3GAL4
PRH2
PRB4
PRB3

D

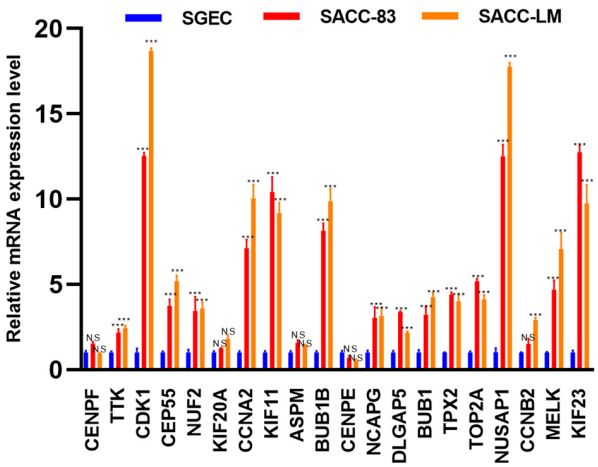


**Figure S1.** DLGAP5 is overexpressed in SACC. A, B: Box plots and principal component analysis (PCA) before and after normalization. C: The PPI network of the DEGs. Nodes represent proteins, edges represent interactions between proteins. Proteins with more interaction were shown in the center of the network. Red represents up-regulated genes, blue represents down-regulated genes, and yellow indicates the top 20 proteins in terms of degree. D: mRNA expression of the above twenty genes in salivary gland epithelial cells, SACC-83, and SACC-LM. The data are presented as the means ± SD. *P < 0.05; **P < 0.01; ***P < 0.001 and ****P < 0.0001, one-way ANOVA.